Magnetic behavior and magnetocaloric effect of neodymium-based amorphous alloy

Stéphane Gorsse, Glenn Orveillon, Bernard Chevalier

Magnetic behaviour and magnetocaloric effect of neodymium-based amorphous alloy

S. Gorsse [a)], G. Orveillon, B. Chevalier

Institut de Chimie de la Matière Condensée de Bordeaux,

ICMCB, CNRS, Université Bordeaux 1

87 Av. Dr A.Schweitzer, 33608 PESSAC Cedex, France

Abstract

The $Nd_{49}Al_{13}Ni_{38}$ amorphous alloy has been prepared by melt-spinning in the form of ribbons. Its magnetic properties have been investigated via superconducting quantum interference device magnetometry and its magnetic phase diagram was established. Hysteresis and temperature-dependent magnetization measurements show the occurrence of a re-entrant spin glass behaviour on cooling. With increasing applied field, the spin-freezing temperature decreases and disappears at very high field, and the Curie temperature increases, broadening the temperature range of the ferromagnetic state. The resulting magnetocaloric effect (MCE) was evaluated and compared to others interesting magnetic refrigerant materials.

a) Corresponding author – gorsse@icmcb-bordeaux.cnrs.fr

1. Introduction

Magnetocaloric effect (MCE) consists in temperature change of magnetic materials upon the application of a magnetic field. MCE attracts very much attention due to its potential application in environmentally-friendly and high energy efficiency magnetic refrigeration [1]. The rejection and absorption of heat is accomplished by adiabatic temperature change upon magnetization and demagnetization of the magnetic refrigerant. Families of magnetic materials which exhibit large MCE value resulting on a large field-induced entropy change include rare-earth (RE) intermetallics (REM_2 where M = Al, Co and Ni) and their hydrides, and manganites ($RE_{1-x}M_xMnO_3$ where M = Ca, Sr and Ba) [2]. Recently, magnetocaloric effect of Fe- [3, 4, 5, 6, 7, 8, 9, 10, 11, 12,], Co- [13], Gd-based [14, 15, 16, 17] and Pd- [18] amorphous alloys have been examined because they display interesting properties for a suitable magnetic refrigerants, e.g. a high electric resistivity that decreases eddy current losses, a tuneable ordering temperature, high corrosion resistance and outstanding mechanical properties.

Amorphous alloys can present a large variety of magnetic properties such as paramagnetism, superparamagnetism, superferromagnetism, and spin glass, depending of their method of preparation (e.g. melt-spinning at different cooling rates, copper mold casting, post annealing) and composition. The disordered structure in amorphous ferromagnets gives rise to random isotropic exchange and random anisotropy resulting of local easy axes whose varies randomly in space, instead of having a global anisotropy along crystallographic axes. According to the random anisotropy model [19], the magnetic behaviour can dramatically be affected by the random anisotropy; depending on its strength disordered phases can exhibit soft or hard magnetic behaviour [20]. Having a magnetic hysteresis reduced to nullity is

particularly interesting for magnetic refrigeration in which energy losses during magnetization/demagnetization cycles must be minimized.

The strength of the random anisotropy and, in consequence, the magnetic properties and MCE of amorphous alloys can be tailored via the choice of the RE solvent element. In RE compounds the magnetic anisotropy results of the spin orbit coupling and depends on the J state of the RE ion. In this perspective, we investigate the properties of a series of RE-Al-Ni amorphous alloys with RE = La, Ce, Nd, Sm, Gd and Dy because of their different J states and magnetic moments. In this paper, we present the magnetic properties and the MCE properties of $Nd_{49}Al_{13}Ni_{38}$ amorphous alloy.

2. Experiment

The alloy composition, $Nd_{49}Al_{13}Ni_{38}$, was designed based on topologic and thermodynamic criteria [21] to ensure a good glass forming ability. The master alloy was prepared by melting precisely weighed amounts of high purity elements Nd (99.9%), Al (99.999%) and Ni (99.995%), in a levitation-furnace. Melting was carried out in a water-cooled copper crucible under a purified argon atmosphere and performed several times to achieve good homogeneity. The amorphous alloy is produced in the form of ribbons by single-roller melt-spinning technique with a circumferential speed of 40 m/s in a purified argon atmosphere.

The amorphous state of the melt-spun ribbon was verified by X-ray diffraction (XRD) and differential scanning calorimetry (DSC).

In order to gain a detailed picture of the magnetic properties of $Nd_{49}Al_{13}Ni_{38}$ melt-spun ribbons, we have measured the temperature and field dependence of dc magnetic susceptibilities. These measurements were performed using a superconducting quantum

interface device (SQUID) magnetometer. Heat capacity was also measured with a Physical Properties Measurement System (PPMS) from Quantum Design in temperature range of 1.8-300 K.

3. Results and discussion

The XRD pattern of the $Nd_{49}Al_{13}Ni_{38}$ melt-spun ribbons is shown in **Figure 1**. Only two broad diffraction peaks are observed which indicates a fully amorphous structure. The occurrence of a glass transition at 524 K further confirms the amorphous nature of the sample (**Fig. 2**).

Plots of the ratio H/M (H, the applied field, and M, the magnetization) as a function of the temperature (**Fig. 3**), and at various applied field ($\mu_0 H$) ranging from 0.005 T to 1 T, shows that the $Nd_{49}Al_{13}Ni_{38}$ amorphous alloy obeys to a Curie–Weiss law at high temperature with a paramagnetic Curie temperature $\theta_p \approx 15$ K and an effective moment μ_{eff} of 3.46 μ_B/Nd. This is very close to the expected value of 3.62 μ_B for Nd^{3+} ions which suggests, together with the positive value of θ_p, a ferromagnetic (FM) spin coupling between RE ions. With decreasing temperature, the ratio H/M starts to deviate from the Curie-Weiss behaviour at the temperature $T_d < 30$ K depending on the applied field. This deviation reflects the establishment of short range exchange interactions giving rise to small correlated volume, i.e. magnetic clusters with a correlation length that increases as the temperature decreases below T_d.

Figure 4 presents the *M(H)* magnetic loops at various temperatures after zero field cooling (ZFC) and the **inset** shows the first magnetization curves at various temperatures. At

270 K, the magnetism can be described with paramagnetism (PM). At 30 and 15 K, the S-shape of the magnetisation loop with no coercivity is typical of superparamagnetism (SPM) - this behaviour is confirmed below from the analysis of the M vs H/T data using the Langevin function. At 9 K, the behaviour is characteristic of ferromagnetism (FM) with an increasing coercivity as the temperature decreases. The $Nd_{49}Al_{13}Ni_{38}$ melt-spun ribbon is a soft magnet at 9 K and a harder magnet at 1.8 K and 3 K with coercivity of 0.3025 and 0.1100 T, and remanence of 17.3 and 11.7 Am^2/kg, respectively. In the inset of Figure 4, one can also see a decrease of the permittivity as the temperature is lowered. Higher coercivity and lower permittivity at low T reveal the presence of a magnetic anisotropy due to the L state of Nd^{3+}. Even at 4.6 T, complete saturation is never achieved which can be attributed to the progressive flipping of spins to a ferromagnetic alignment and suggests the presence of antiferromagnetic interactions between Nd^{3+} ions. In a disordered system containing RE, the variation of local environments and distances can cause the intensity and sign of the RKKY exchange interactions to fluctuate in space, and, as a consequence, the spins in a given magnetic cluster are not necessary all ferromagnetically aligned in the same direction.

In **Figure 5**, the zero-field-cooled (ZFC) and field-cooled (FC) magnetization curves *M(T)* of the amorphous alloy show a paramagnetic-ferromagnetic phase transition at T_C = 11-16 K, and a thermomagnetic irreversibility between ZFC and FC conditions at T_{irr} = 5-9 K. This difference at low T between ZFC and FC curves is attributed to the local random magnetic anisotropy. The irreversibility is below approximately 10 K, depending of the applied field. Above this bifurcation, ZFC and FC curves superimpose perfectly while below, the ZFC branch decreases rapidly and the FC branch increases to a plateau. The maxima of the ZFC curve decreases to lower T with increasing field from 0.005 to 0.1 T, and matches with the temperature of irreversibility, T_{irr}. At higher field ($\mu_0 H$ = 1 T), ZFC and FC curves

superimpose in the whole temperature range from 1.8 K to 300 K and encounter a plateau below 10 K. Possible origins of this overall behaviour include surface-spin-glass freezing, cooperative freezing of interacting magnetic clusters (superferromagnetism), re-entrant spin glass transition or superparamagnetism blocking. Xu et al. [22] observed for an amorphous alloy with similar composition (i.e. $Nd_{53}Al_{15}Ni_{32}$) and prepared in the same way, that the ZFC peak around 10 K moves to higher temperature with increasing frequency in ac susceptibility. This suggests a spin glass with re-entry [23], i.e. the spin glass phase develops from a FM state and it re-enters the frozen disordered phase out of another paramagnetic disordered phase (PM). More details of the temperature dependence of the magnetisation are given by the derivative of M (inset of **Fig. 5**). The *dM/dT* vs *T* curves were plotted for each applied field H. To facilitate the lecture, logarithm scale is used for the temperature axis. The ordering temperature T_c for PM to FM transition and the freezing temperature T_f for FM to SG transition were determined at the kinks (Table 1). The bifurcation of ZFC and FC *dM/dT* curves denotes the progressive freezing of spins or group of spins (clusters) below T_{irr}. **Figure 6** shows that the field dependence of T_f and T_{irr} follow the Almeida-Thouless (AT) line with a $H^{1/2}$ law which has also been observed in re-entrant SG systems [24] and predicted by the Sherrington-Kirkpatrick model of SG [25].

The magnetic ordering transition observed on the M(T) curves is also visible in the temperature dependence of the heat capacity, $C_p(T)$, shown in **Figure 7**. Only one small anomaly around 10 K is observed, which is characteristic of a second order phase transition. This anomaly shifts to higher temperature with increasing the applied field, from 10 K for $\mu_0 H = 0$ T to 12 K for $\mu_0 H = 1$ T (**inset of Fig. 7**). These values are close to T_c obtained above from magnetisation curves (**Fig. 5** and **Table 1**).

From the above results we can draw the following picture to explain the overall magnetic behaviour of the $Nd_{49}Al_{13}Ni_{38}$ amorphous alloy. At high temperature, there is one PM phase made of weakly interacting Nd^{3+}; the thermal dependence of the magnetization is well reproduced by the Brillouin function (**Fig. 8**). Between T_d and T_C, the competition between ordering due to exchange interaction and the disordering effect of temperature gives rise to the formation of ordered magnetic clusters embedded into a PM matrix, when short range exchange for a group of spins becomes higher than kT. A quantitative analysis using the Langevin function confirms this description and shows an increase of the number of clusters as the temperature is lowered (Fig. 8). On cooling, these correlated volumes grow resulting of an increase of the correlation length up to the infinite magnetic cluster with wandering axes. Below T_{irr}, the hysteretic behaviour results of the progressive broken up of the magnetically ordered phase by the local anisotropy into frozen and randomly oriented clusters. The presence of coercivity indicates that the anisotropic clusters formed below T_{irr} have a size comparable to the exchange coupling correlation length. As the temperature is kept decreasing less and less spin can overcome the local anisotropy, and below T_f spins are frozen along their local anisotropy axes.

The H-T phase diagram (**Fig. 9**) consists of two disordered phases (PM and SG) and ordered magnetic clusters, separated by binary regions in which magnetically correlated volumes are formed into one of the disordered phase.

The resulting magnetocaloric response of the $Nd_{49}Al_{13}Ni_{38}$ amorphous alloy has been derived from Maxwell relation by integrating over the magnetic field:

$\left(\frac{\partial S}{\partial M}\right)_T = \left(\frac{\partial M}{\partial T}\right)_H$ where *S* represents the magnetic entropy.

The magnetic entropy change, ΔS_M, produced by the variation of a magnetic field from 0 to H_{max} is given by

$$\Delta S_M(T,H) = \int_0^{H_{\max}} \left(\frac{\partial M}{\partial T}\right)_H dH$$

and the adiabatic temperature change, ΔT_{ad}, linked to MCE can be expressed as $\Delta T_{ad} = -\left(T/C_0(T)\right)\Delta S_M$.

Figure 10 shows the temperature dependence of the magnetic entropy change, $\Delta S_M(T)$, corresponding to an applied field H of 1 T. The behaviour shows several remarkable features. There are two peaks corresponding to the SG to FM transition at T_f and the FM to PM transition at T_c, with a positive and negative value, respectively. The peak entropy change at T_c is ΔS_M = -1.6 J.kg^{-1}.K^{-1}, corresponding to the adiabatic temperature change ΔT_{ad} = 5.4 K, which compare well with other known MCE materials (**Table 2**). The FM to PM transition in the $Nd_{48}Al_{13}Ni_{38}$ amorphous alloy produces a broad peak in the magnetic entropy change (**Fig. 10**). This characteristic, resulting of the disordered structure of the material, is interesting since it enhances the refrigerant capacity [26]. T_c is lowered due to the disorder effect that significantly reduces the electron mean free path and in consequence decreases the RKKY coupling at smaller length scale.

4. Conclusion

The magnetic behaviour of the $Nd_{49}Al_{13}Ni_{38}$ amorphous alloy goes from paramagnetic, ferromagnetic to spin-glass upon cooling. It is a soft magnet at 9 K and becomes a hard magnet with higher coercivity at lower temperature. This overall behaviour originates from the formation of magnetic clusters resulting on the competition between the development of short-range spatial magnetic ordering and the disordering effect of the

random magnetic anisotropy. Given its H-T magnetic phase diagram, exhibiting a large panel of magnetic phases (PM, FM, and SG), the $Nd_{49}Al_{13}Ni_{38}$ amorphous alloy provides a good prototype to compare the effect of the strength of the random anisotropy since other choices for the RE element should give rise to modifications of the H-T diagram with enlargement of specific phase fields and reduction of others. In term of MCE, ΔS_m of $Nd_{49}Al_{13}Ni_{38}$ compares well with others amorphous materials. It appears that, in addition of heat treatments that can be performed on the amorphous to produce nanocomposite structures, tuning the strength of the random anisotropy could be another degree of freedom allowing to tailor the magnetic properties and MCE of amorphous alloys.

5. Acknowledgements

Financial support from the European Office of Aerospace Research and Development through Research Task FA8655-07-M-4003 is greatly appreciated. SG wishes to thank O. Senkov for DSC experiments.

References

1 J. Glanz, Science 279, 2045 (1998).

2 K.A. Gscheidner, V.K. Pechersky, and A.O. Tsokol, Rep. Prog. Phys. 68, 1479 (2005).

3 D. Wang, K. Peng, B. Gu, Z. Han, S. Tang, W. Qin, and Y. DU, J. Alloys Compd. 358, 312 (2003).

4 S. Atalay, H. Gencer, and V.S. Kolat, J. Non-Cryst. Solids 351, 2373 (2005).

5 S.G. Min, K.S. Kim, S.C. Yu, H.S. Suh, and S.W. Lee, J. Appl. Phys. 97, 10M310 (2005).

6 V. Fransco, J.S. Blazquez, C.F. Conde, and A. Conde, Appl. Phys. Lett. 88, 042505 (2006).

7 F. Johnson and R.D. Shull, J. Appl. Phys. 99, 08K909 (2006).

8 V. Franco, J.S. Blazquez, and A. Conde, J. Appl. Phys. 100, 064307 (2006).

9 V. Franco, J.M. Borrego, A. Conde, and S. Roth, Appl. Phys. Lett. 88, 132509 (2006).

10 V. Franco, J.M. Borrego, C.F. Conde, A. Conde, M. Stoica, and S. Roth, J. Appl. Phys. 100, 083903 (2006).

11 V. Franco, J.S. Blazquez, M. Millian, J.M. Borrego, C.F. Conde, and A. Conde, J. Appl. Phys. 101, 09C503 (2007).

12 S.G. Min, K.S. Kim, S.C. Yu, and K.W. Lee, Mat. Sci. Eng. A 449-451, 423 (2007).

13 P. Didukh and A. Slawska-Waniewska, J. Magn. Magn. Mater. 254/255, 407 (2003).

14 M. Foldeaki, R. Chachine, B.R. Gopal, T.K. Bose, X.Y. Liu, and J.A. Barclay, J. Appl. Phys. 83, 2727 (1998).

15 Q. Luo, D.Q. Zhao, M.X. Pan, and W.H. Wang, App. Phys. Lett. 89, 081914 (2006).

16 L. Si, J. Ding, Y. Li, B. Yao, and H. Tan, Appl. Phys. A 75, 535 (2002).

17 B. Chevalier, J.-L. Bobet, J. Sanchez Marcos, J. Rodriguez Fernandez, and J.C. Gomez Sal, Applied Physics A, 80, 601 (2005).

18 T.D. Shen, R.B. Schwarz, J.Y. Coultier, and J.D. Thompson, J. Appl. Phys. 91, 5240 (2002).

19 R. Harris, M. Plisschke, and M.J. Zuckermann, Phys. Rev. Lett. 31, 160 (1973).

20 R. Alben, J.J. Becker, M.C. Chi, J. Appl. Phys. 49, 1653 (1978).

21 G. Orveillon, O.N. Senkov, J.-L Soubeyroux, B. Chevalier, and S. Gorsse, Adv. Eng. Mater. 9, 483 (2007).

22 F. Xu, X. Wu, Y. Du, C. Cui, and G. Chen, J. Appl. Phys. 99, 08B524 (2006).

23 J. A. Mydosh, Spin Glasses (Taylor and Francis, London, 1993).

24 Y.T. Wang, H. Y. Bai, M. X. Pan, D. Q. Zhao, and W. H. Wang, Phys. Rev. B 74, 064422 (2006).

25 J. R. L. de Almeida and D. J. Thouless, J. Phys. A 11, 983 (1978).

26 M. E. Wood and W. H. Potter, Cryogenics 25, 667 (1985).

Tables

Table 1: Freezing temperature (T_f), temperature of irreversibility (T_{irr}), ferromagnetic transition (T_C) and deviation from the Curie-Weiss law (T_d) obtained at various applied fields for the $Nd_{49}Al_{13}Ni_{38}$ amorphous alloy.

μ_0.H (T)	T_f (K)	T_{irr} (K)	T_c (K)	T_d (K)
0.005	8.7	9.5	11.5	20.0
0.015	7.1	8.7	12.0	20.0
0.025	6.0	7.8	12.0	20.0
0.1	3.6	5.5	13.2	21.5
1	-	-	15.8	26.0

Table 2: Magnetic entropy change upon applying a field H at various materials and related parameters.

Amorphous alloys	T_C (K)	ΔH (T)	$-\Delta S_M$ (J kg^{-1} K^{-1})	ΔT_{ad} (K)	References
$Nd_{49}Al_{13}Ni_{38}$	15.8	1	1.6	5.4	Present work
Fe-based	125 - 490	1	0.2 – 1.4	-	[3 – 12]
Pd-based	94	5	0.6		[18]
RE-based	30 - 90	5	9 - 12		[14 – 17]

Figures captions

Figure 1: DRX pattern of the melt-spun ribbon of $Nd_{49}Al_{13}Ni_{38}$.

Figure 2: Heat flow vs. temperature curves of the $Nd_{49}Al_{13}Ni_{38}$ amorphous alloy at the heating rate of 40 K/min. The exothermic reactions are up.

Figure 3: H/M ratio plots of the $Nd_{49}Al_{13}Ni_{38}$ amorphous alloy at various applied field ($\mu_0 H$ = 0.1 and 1 T). The line represents the Curie-Weiss law at high temperatures (R^2 = 0.999).

Figure 4: Magnetic hysteresis loops *M(H)* of the $Nd_{49}Al_{13}Ni_{38}$ amorphous alloy at various temperatures (T = 270, 30, 15, 9, 3 and 1.8 K). The inset shows the first magnetisation curves at the same temperatures.

Figure 5: Zero-Field-Cooled (ZFC - open symbols) and Field-Cooled (FC – full symbols) magnetization curves *M(T)* of the $Nd_{49}Al_{13}Ni_{38}$ amorphous alloy at various applied field ($\mu_0 H$ = 0.005, 0.015, 0.025, 0.1, and 1 T). The inset represents the ZFC-FC derivates of magnetization *dM/dT* vs *T* for each applied field H. A log-scale is used for *T*.

Figure 6: Field dependence of freezing temperature (T_f) and temperature of irreversibility (T_{irr}). The lines represent the Almeida-Thouless $H^{1/2}$ dependence law.

Figure 7: Specific heat capacity at constant pressure of the $Nd_{49}Al_{13}Ni_{38}$ amorphous alloy without (open circles) and with (full triangles) applied magnetic field of $\mu_0 H$ = 1 T. The line

represents the Debye heat capacity model. The inset figure is the C_P/T *vs* T plot showing more clearly the magnetic transition around 10 K.

Figure 8: Magnetization vs H/T for T = 15 and 30 K, and curves of the Langevin function. At 15 and 30 K, there are two phases, i.e. the ordered magnetic clusters and the PM phase described with the Langevin function and the Brillouin function, respectively. The fits give 50 and 10% for the proportion of clusters into the PM phase, and 100 and 30 μ_B for the cluster moment at 15 and 30 K, respectively. Inset figure shows the good fit at 270 K with the Brillouin function.

Figure 9: Magnetic phase diagram (H-T) of the $Nd_{49}Al_{13}Ni_{38}$ amorphous alloy constructed from present results. PM, SPM, FM, CG and SG stand for paramagnetic, superparamagnetic, ferromagnetic, cluster-glass and spin-glass domain, respectively. The various lines represent the characteristic temperatures T_d, T_C, T_{irr}, T_f which are summarized Table 1.

Figure 10: Temperature dependence of the magnetic entropy of the $Nd_{49}Al_{13}Ni_{38}$ amorphous corresponding to $\mu_0\Delta H$ = 1 T and calculated from equation 2.

Figures

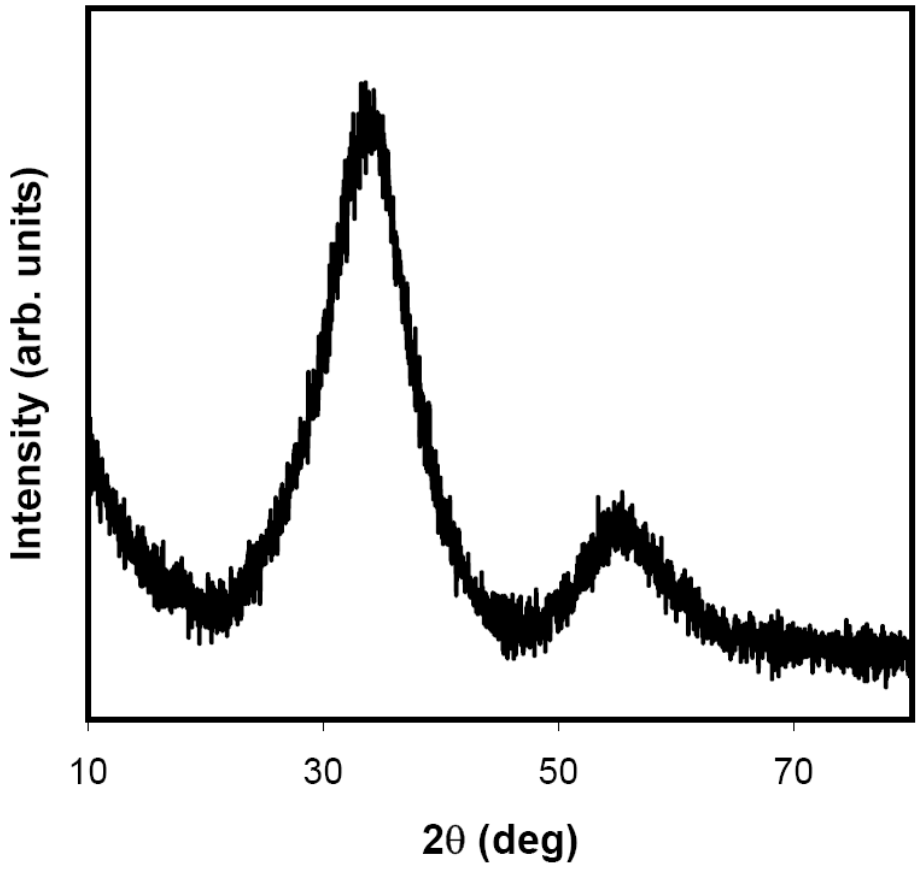

Figure 1:

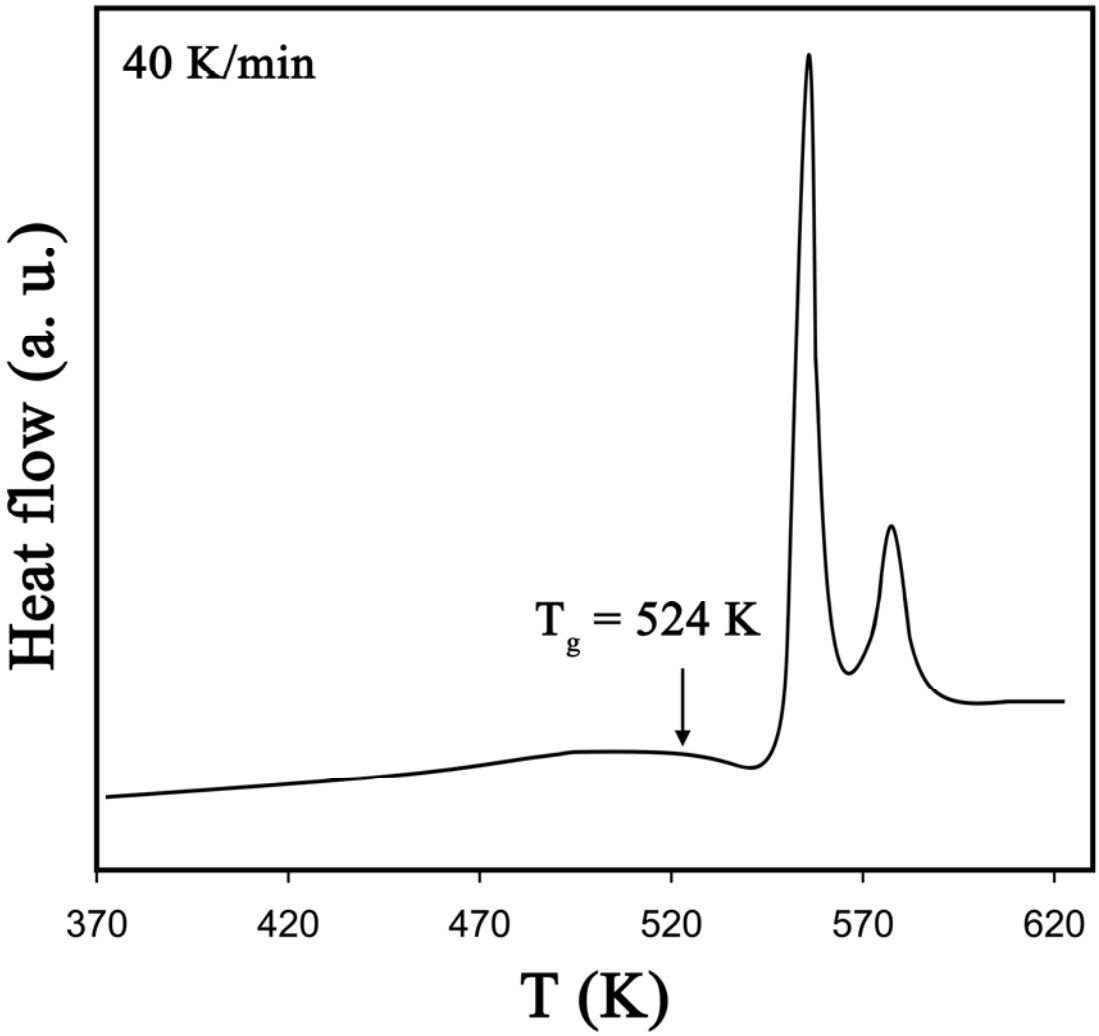

Figure 2:

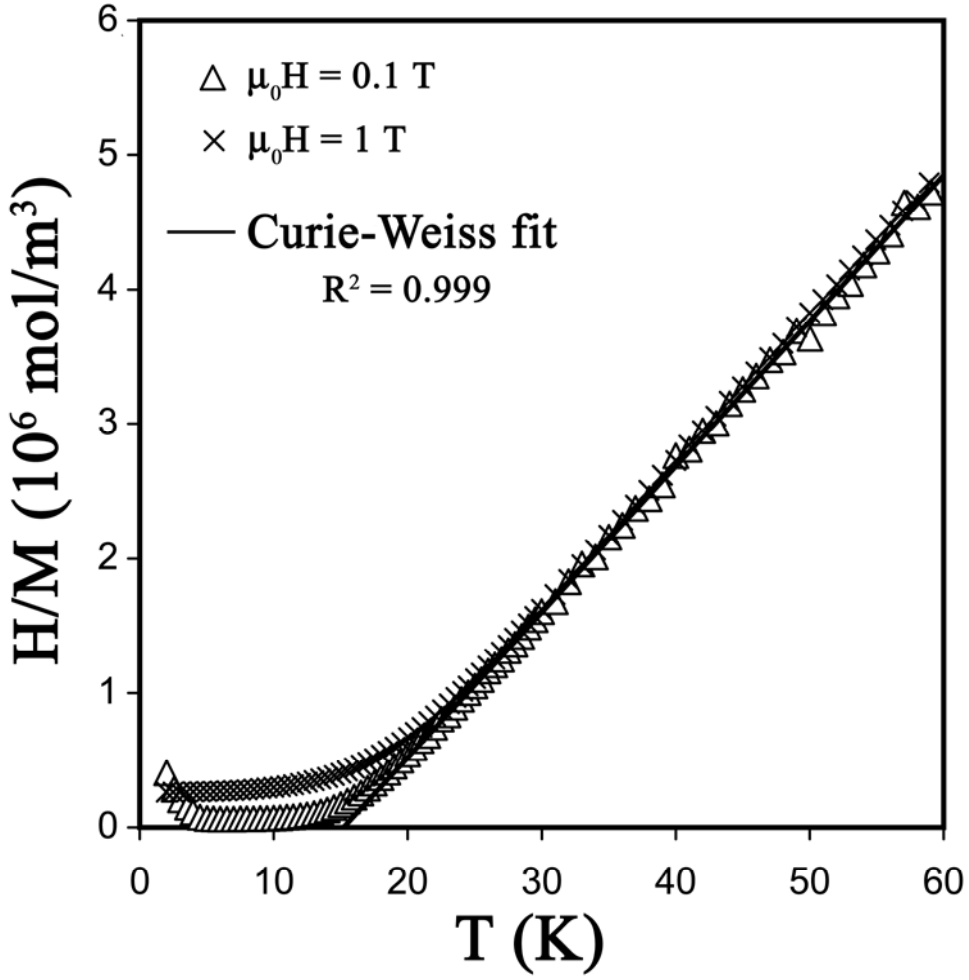
△ μ0H = 0.1 T
× μ0H = 1 T
Curie-Weiss fit
R2 = 0.999
H/M (10^6 mol/m^3)
T (K)
0
1
2
3
4
5
6
0
10
20
30
40
50
60

Figure 3:

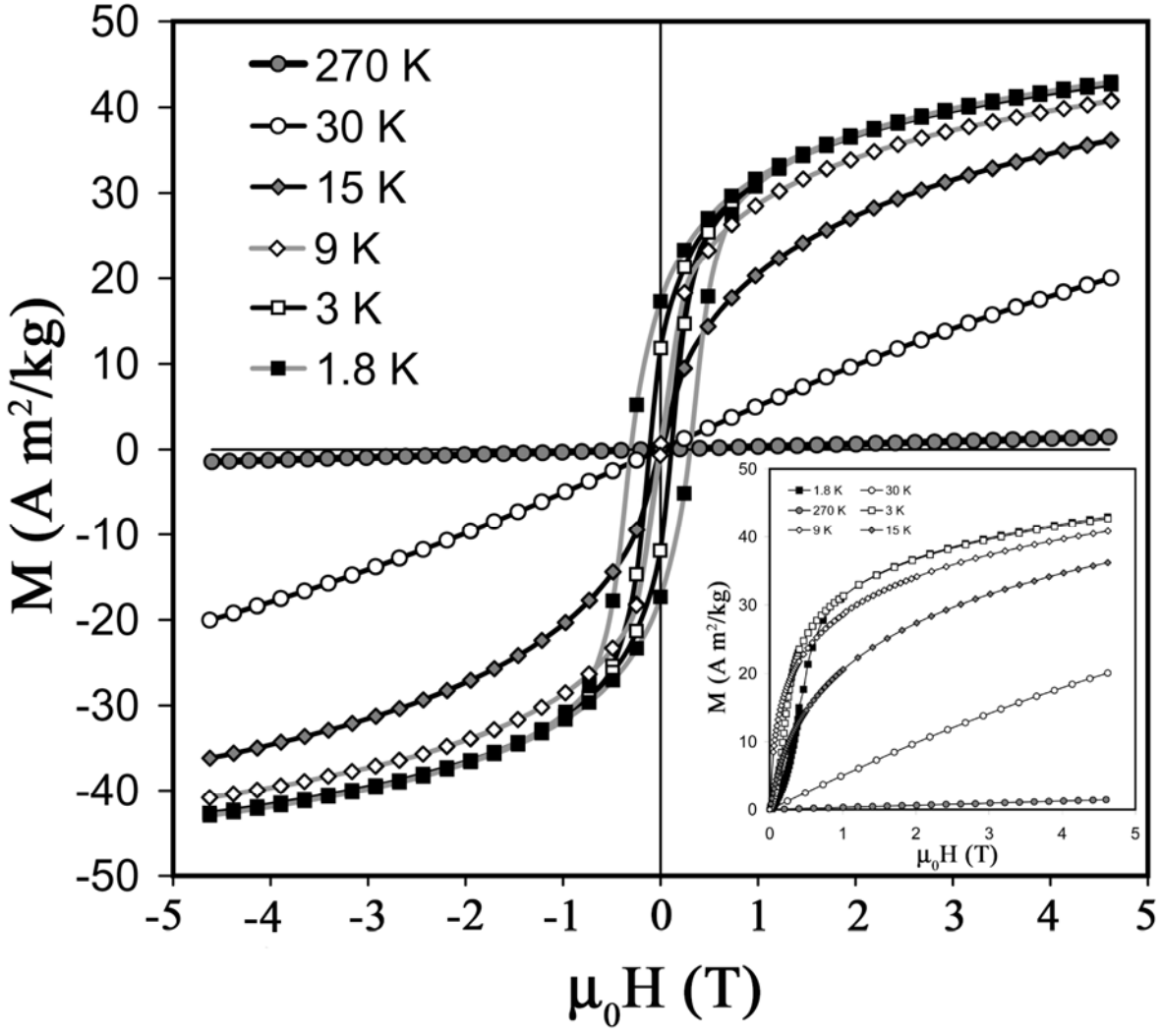
270 K
30 K
15 K
9 K
3 K
1.8 K
M (A m²/kg)
μ0H (T)
1.8 K
30 K
270 K
3 K
9 K
15 K
M (A m²/kg)
μ0H (T)

Figure 4

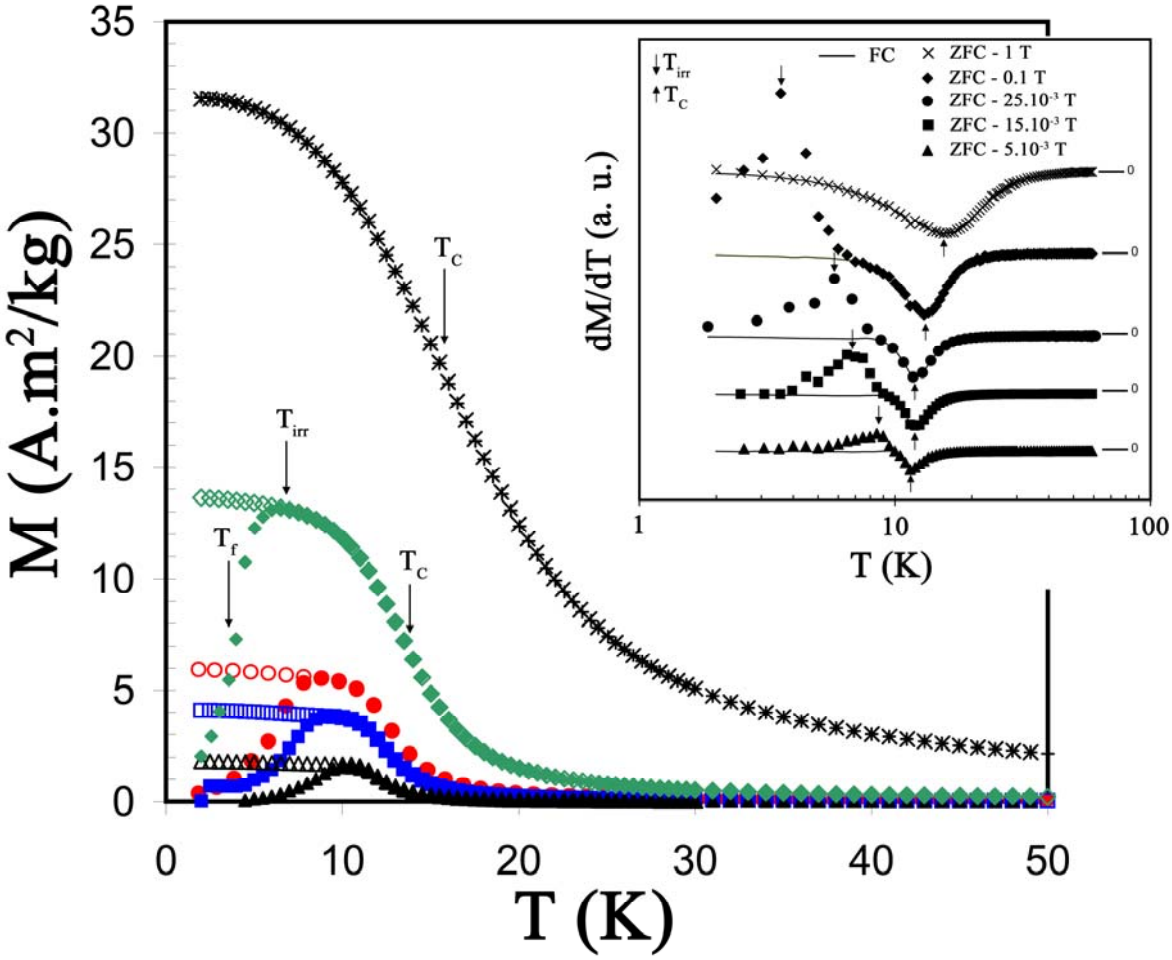
M (A.m²/kg)
T (K)
T_C
T_irr
T_f
T_C
dM/dT (a. u.)
T (K)
FC
ZFC - 1 T
ZFC - 0.1 T
ZFC - 25.10⁻³ T
ZFC - 15.10⁻³ T
ZFC - 5.10⁻³ T
T_irr
T_C

Figure 5:

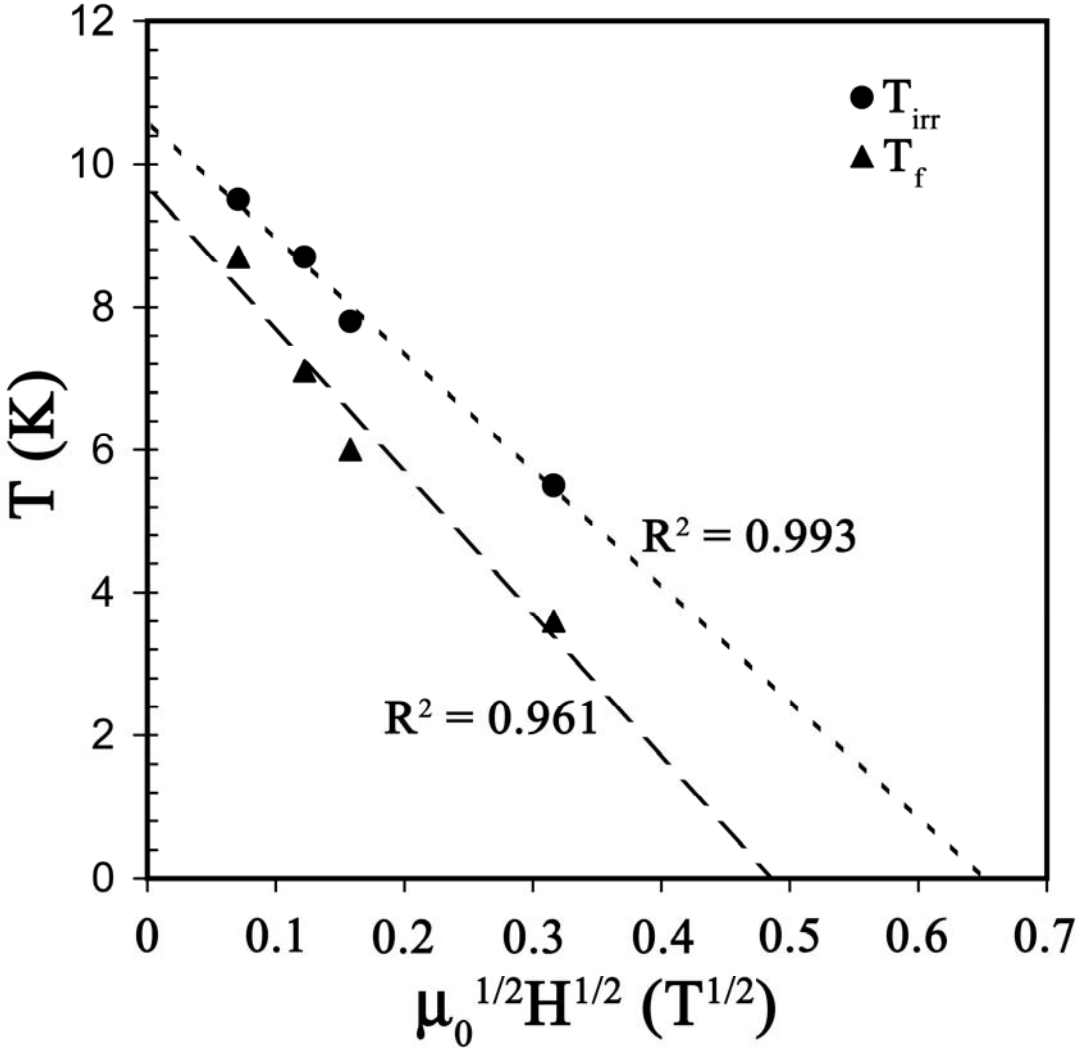
12
10
8
6
4
2
0
T (K)
0
0.1
0.2
0.3
0.4
0.5
0.6
0.7
μ0 1/2H1/2 (T1/2)
Tirr
Tf
R2 = 0.993
R2 = 0.961

Figure 6

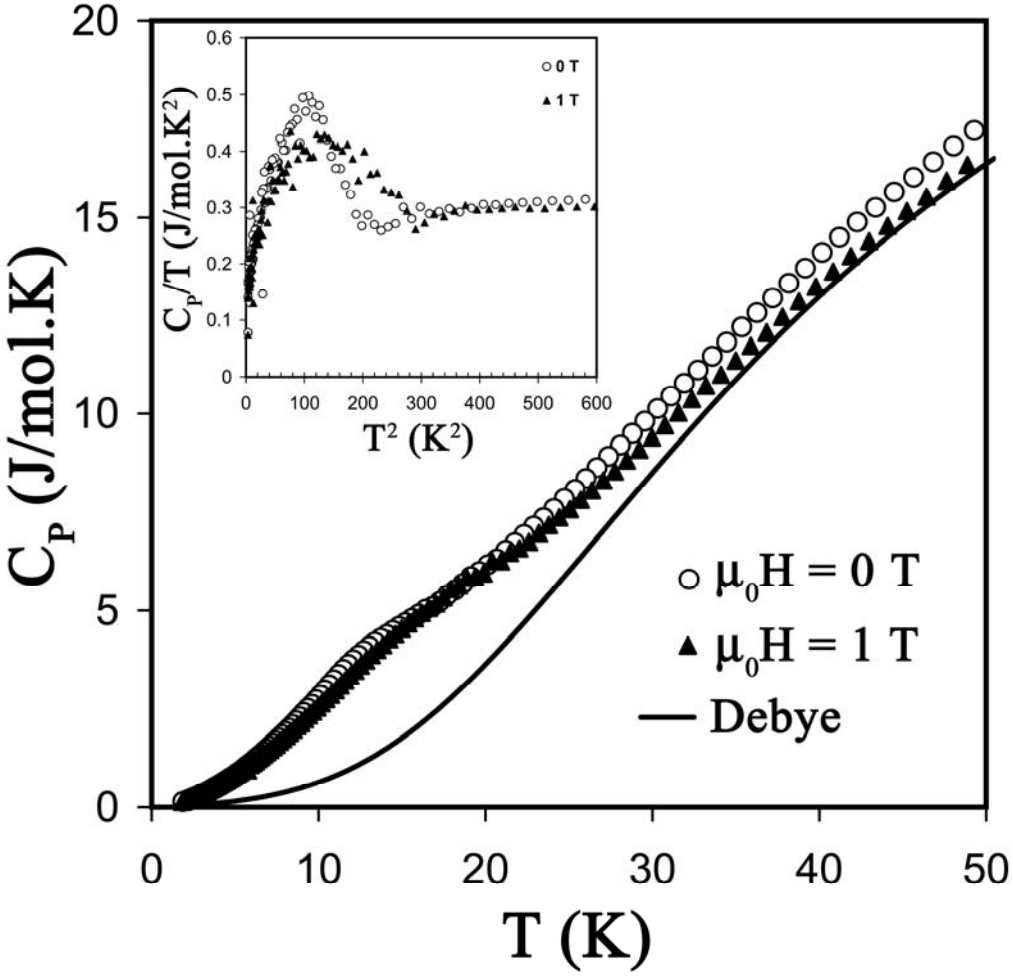

Figure 7

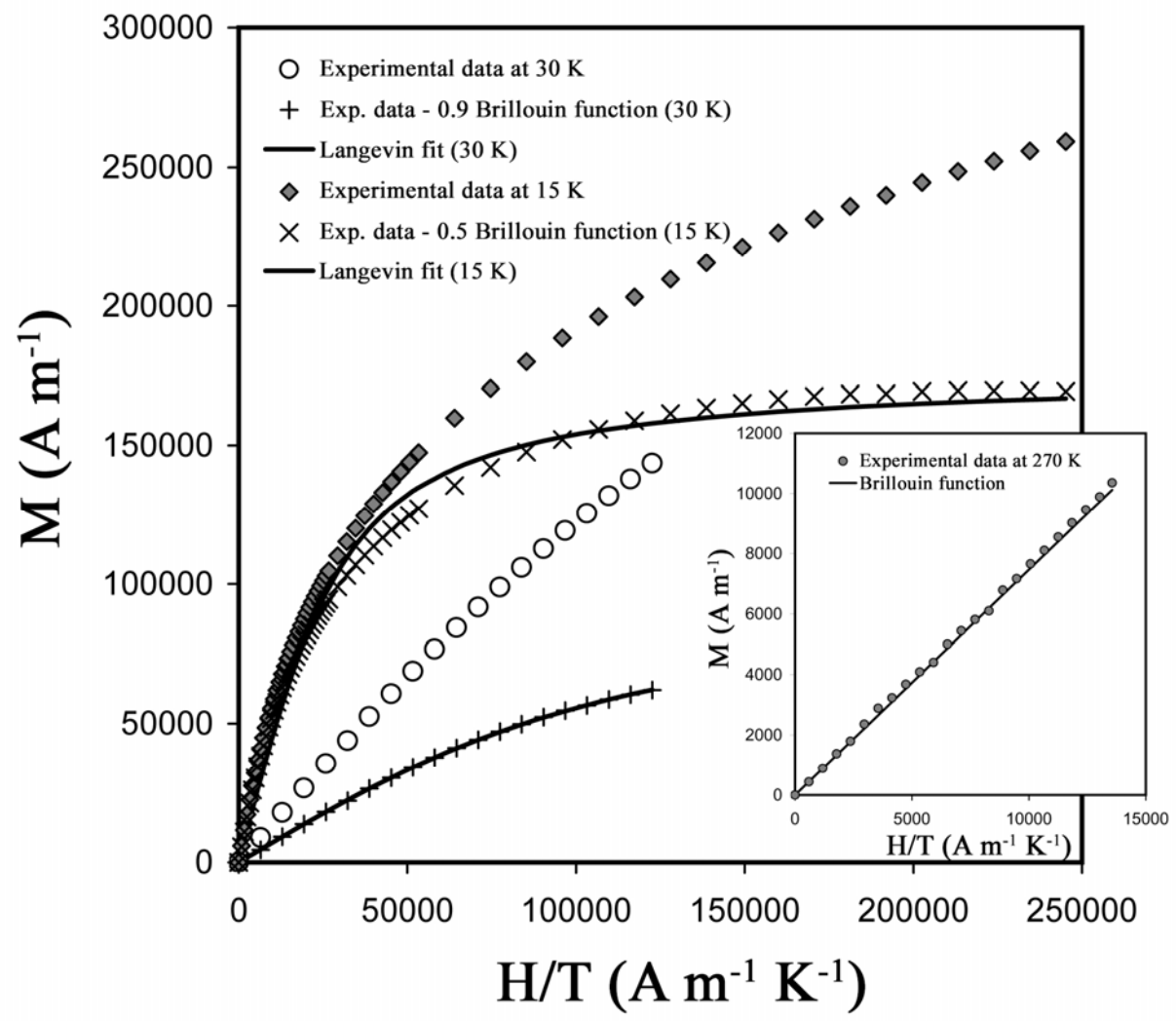
Experimental data at 30 K
Exp. data - 0.9 Brillouin function (30 K)
Langevin fit (30 K)
Experimental data at 15 K
Exp. data - 0.5 Brillouin function (15 K)
Langevin fit (15 K)
M (A m-1)
H/T (A m-1 K-1)
0
50000
100000
150000
200000
250000
300000
Experimental data at 270 K
Brillouin function
M (A m-1)
H/T (A m-1 K-1)
0
2000
4000
6000
8000
10000
12000
5000
15000

Figure 8 :

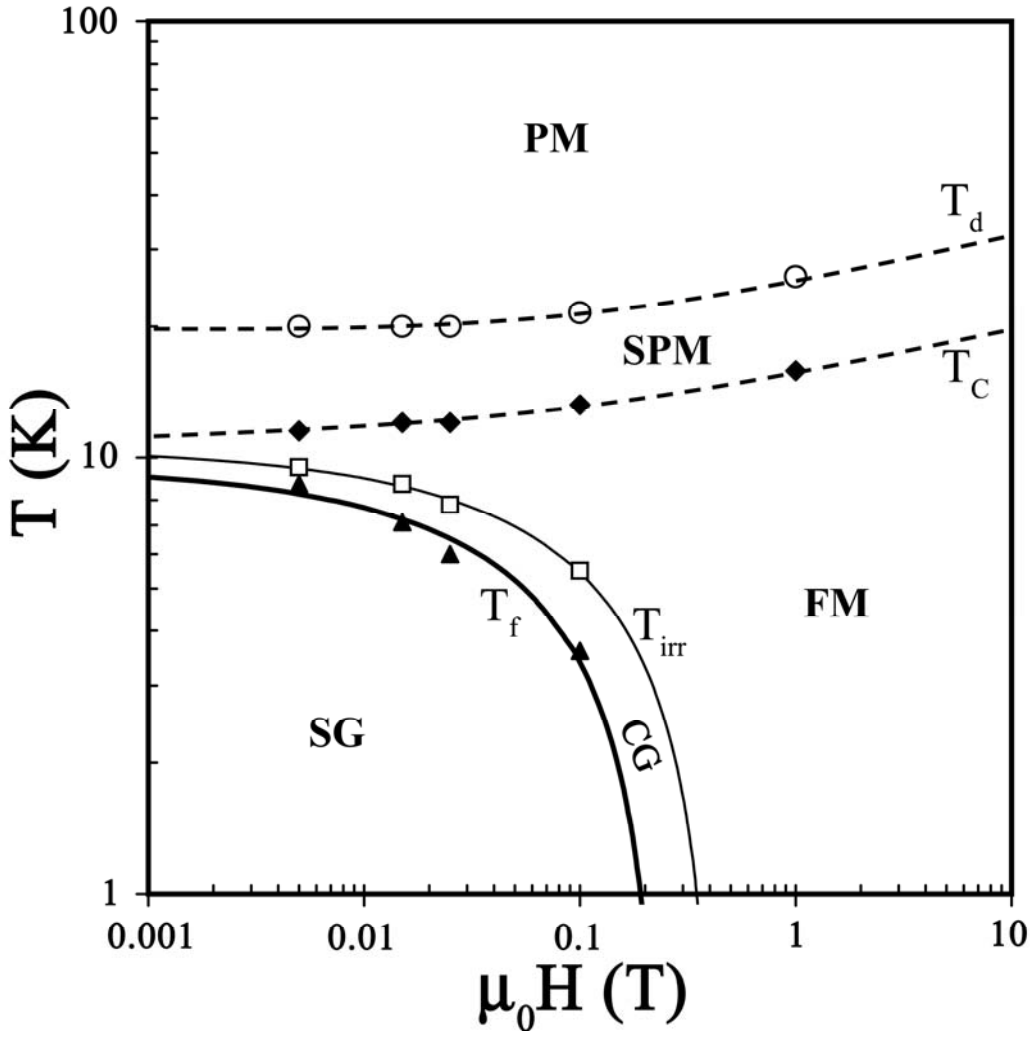

Figure 9

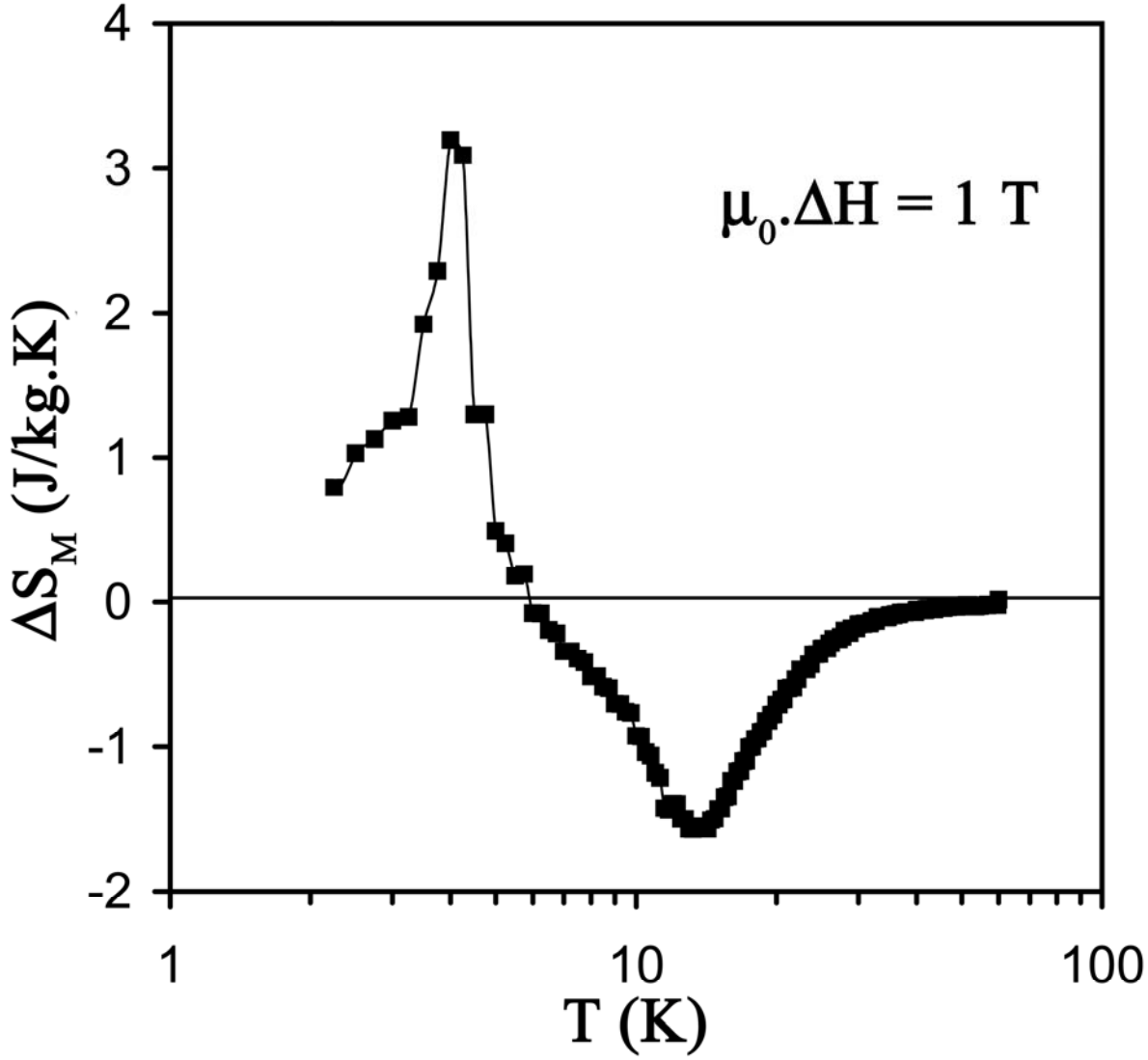

Figure 10